GeoArabia, Vol. 12, No. 1, 2007
Gulf PetroLink, Bahrain

Fault growth and coalescence: insights from numerical modelling and sandbox experiments

Jacek B. Filbrandt, Pascal D. Richard and Raymond Franssen

ABSTRACT

Displacement of strata varies along the strike of faults. This has important implications for the hydrocarbon industry, since for example this affects the occurrence and distribution of fractures along faults in a reservoir and can influence the sealing capacity of faults. As faults grow, neighbouring faults will interact with each other and eventually connect or coalesce. Geometrical fault growth models for coalescence are used to explain a large part of the observed spread of one order of magnitude in Length and Maximum Throw in natural examples of fault populations. Numerical modelling indicates that coalesced (merged) faults tend to return to their steady state growth evolution by accumulating displacement more rapidly than increasing in length, if no further coalescence occurs. Therefore, repetitive coalescence leaves faults "under-displaced" and results in a considerable spread in Length and Maximum Throw. To confirm and support these observations, a series of sandbox experiments was performed, which help improve our understanding of fault growth processes. The fault geometries observed in these models reflect geometries in natural examples, for example in the Natih Formation of Al Jabal al Akhdar in Oman. With increasing strain, repetitive coalescence takes place at all scales. After linkage, a new, coalesced fault behaves as a single, linked segment and accumulates more displacement than increasing length during an increment of strain. The slope of the best fit line of Length vs. Maximum Throw data for the fault population, in double logarithmic space, steepens with increasing strain and stabilises at about one.

INTRODUCTION

Large intra-plate areas of the Arabian Plate with its numerous oil and gas fields are not considered to be heavily affected by structural deformation. However, the importance of faults and their flow/seal properties, together with the often highly fractured fault damage zones, have been recognised by numerous authors when exploring for new fields or successfully depleting existing reservoirs in the interior of the Arabian Plate from Kuwait to Oman (e.g. Filbrandt et al., 2006; Webb et al., 2000; Sercombe et al., 2004; Johnson et al., 2004; 2005). Lateral changes of displacement along the strike of a fault are often associated with changing fracture densities and properties. Stratigraphic displacement variation along subsurface faults on a local and regional scale has been recognised from the interpretation of 3-D seismic data in the hydrocarbon provinces in the Middle East (e.g. Lange et al., 2006; Johnson et al., 2005; Tamura et al., 2004).

Several geometrical fault growth models have been developed for populations of single faults in field-based and sub-surface studies in recent years to explain observed Length (L)/ Maximum Throw (T_{max}) ratios and trends in fault populations, where the cumulative displacement, T_{max}, is related to the total fault length, L, according to the following expression:

$$T_{max} \; \alpha \; L^C$$

The power law exponent, C, for these empirical growth models has been derived by various workers. Cowie and Scholz (1992) proposed that cumulative slip and fault length maintain a constant ratio, so that C = 1 (here referred to as "Model I") and the L/T_{max} ratio remains constant at all scales. Watterson (1986) proposed that cumulative displacement increases at a faster rate than fault length (where C = 2). In this model (referred to here as "Model II"), the L/T_{max} ratio decreases with fault size. Other authors have proposed intermediate models (Marrett and Allmendinger, 1990; Walsh and Watterson, 1992) in which C = 1.5. However, the process of fault evolution through time has not yet been described directly from measurements.

Cartwright et al. (1995) have noted that faults are often segmented and up to ten coalesced segments have been observed in outcrop, now connected into a through-going fault. These authors first noted the spread in L/T_{max} ratio in such fault populations. The existence of linked fault systems and the inferred physical connection of two or more, initially separate, fault segments due to linkage during fault propagation appear to be a common and well documented process (Cowie and Roberts, 2001; Morewood and Roberts, 2002; Walsh et al., 2002; Shipton and Cowie, 2003). By applying rules derived from existing numerical growth models and studying sandbox experiments, the effect of coalescence can be observed (Figure 1) through time.

It is the aim of this contribution to present the consequences of adopting various single-fault growth models for coalescence in an evolving population through examination of numerical growth models (Filbrandt et al., 1995). Details of the derivation of the incremental growth laws discussed below are presented in the appendix. We also present results of sandbox experiments in which fault growth and coalescence have been studied using a video laser scanner to digitise the surface of the sand-pack. We highlight analogous fault geometries observed in one of the principal hydrocarbon reservoirs of Oman in surface exposures of Al Jabal al Akhdar.

FAULT GROWTH AND STEADY STATE

Rule-based, numerical models for *single faults* have been evaluated by iteration using a simple, incremental approach derived from Cowie and Scholz (1992) and Walsh and Watterson (1992), for example, to simulate fault growth after expanding and recasting their equations. The evolution of fault length and displacement during growth described by the relations above are graphically represented in Figure 1a.

After an initial period of rapid accumulation of displacement on a 'seed' fault, represented by a steep positive gradient, fault propagation trajectories reach steady state growth represented by a straight line in double logarithmic space. For example, for an exponent, C, of 1 the L/T_{max} curve achieves a constant gradient at a length of about 10 m and displacement of 0.02 m. The actual position of the growth curve depends on initial fault "seed" dimensions. The gradient of the (almost) linear, steady-state part of the trajectory is related to the power-law exponent, C, defined above for the single, growing fault. The growth curve evolves towards the same linear segment for all initial conditions given the same power-law exponent (Figure 1a). The rate at which steady-state is reached depends strongly on the power exponent, e.g. many more displacement increments are required to reach steady-state for $C = 2$ than for $C = 0.5$.

FAULT COALESCENCE IN NUMERICAL MODELS

Now, let us assume that two initially, separate but neighbouring faults, both having reached steady-state growth, connect and begin to accumulate displacement together. After linkage, the original stable growth is perturbed: the new fault is 'under-displaced' (cf. Cartwright et al., 1995), i.e. its length is too large in relation to the amount of accumulated displacement, expressed as T_{max} or mean throw on the fault (Figure 1b). Continuing the growth iterations for this new fault in each of the

---

Figure 1 (opposite page): Numerical simulations of fault growth (propagation) and coalescence. The linear segments represent stable or "steady-state" fault growth of single or coalesced faults for different values of the power law exponent (C) in the relationship $T_{max} \alpha L^C$. The curves represent the growth path of an initial fault seed or a coalesced fault that is under-displaced relative to the "target" steady state for a given power law exponent.

(a) Fault growth curves for various growth law power exponents (C) for single faults. The curves are modelled (see Appendix) for assumed initial dimensions of seed fault (Lo) with high length to throw ratios. Irrespective of the value of the power law exponent and L/T_{max} ratio of the initial seed, the faults tend to grow towards the steady-state line governed by the selected value of the power law exponent. Rapid accumulation of throw characterises the first part of the growth curve followed by a relatively rapid increase in fault length.

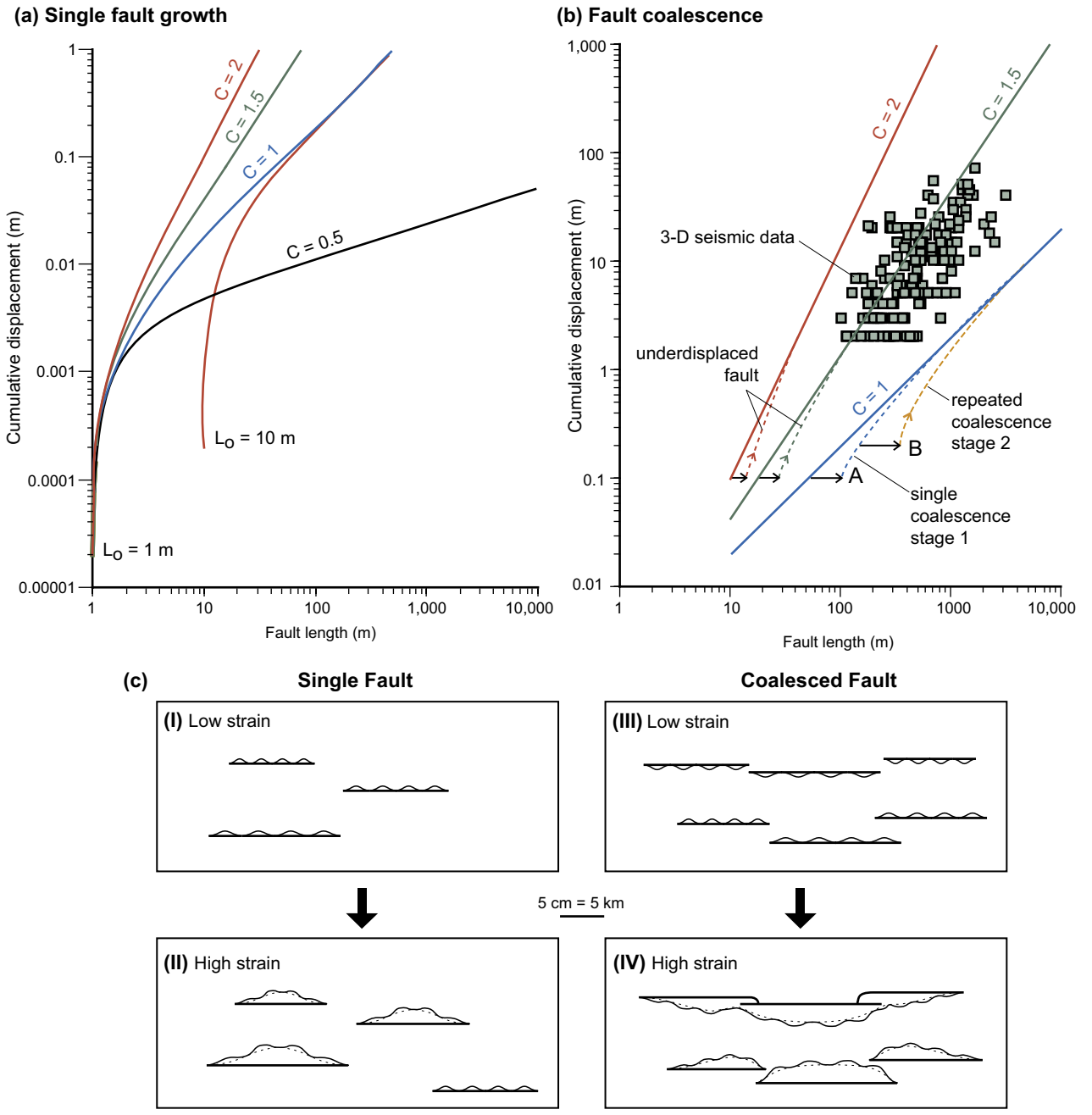

Figure 1 (continued):

(b) Effect of fault coalescence on growth evolution. There is a large spread in L/T_{max} ratio of faults mapped on 3-D seismic data (square symbols) believed to be the result of repeated coalescence events in the fault population (Figure 1c III and 1c IV). Coalescence events cause the newly connected faults to become under-displaced relative to the steady-state growth line represented by a move towards the right in L/T_{max} space i.e. an increase in length with no increase in maximum throw (e.g. A or B). As growth continues with strain, throw accumulates at a faster rate than length on the new, coalesced fault.

(c) The effect of fault seed distribution on the final fault pattern. Single and Coalesced Faults represent end members of the possible distribution of faults and the manner in which they grow with increasing strain. (I) An early, coalescence-dominated phase of growth takes place. Faults reach a given length quickly. Subsequently (II), no interaction takes place. The faults remain isolated. Their throw rapidly increases but not their length. (III) and (IV) represent another end member in which fault seeds are arranged in linear arrays and fault growth is dominated by fault interaction and coalescence at all scales.

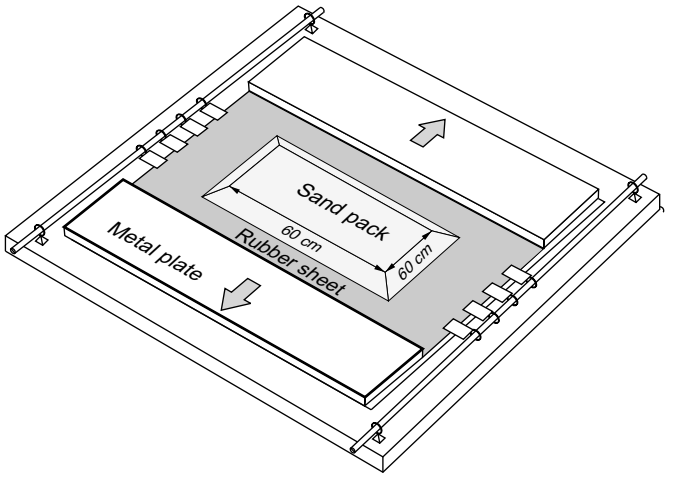

Figure 2: Experimental configuration for homogeneous plane strain extension. A thin rubber sheet (0.2 x 100 x 120 cm) attached to two metal plates lies on a flat horizontal rigid table. The rubber sheet was stretched by withdrawing the metal plates. To maintain a constant sheet length perpendicular to the extension direction, the two other sides of the rubber sheet were fixed to a series of rings sliding along rigid bars.

models, the fault length increases, but once again the 'under-displaced' fault initially accumulates displacement at a greater rate than the corresponding incremental increase in length (compared to the equivalent steady-state growth). However, in all cases, the fault ultimately reaches the steady-state growth trajectory after many tens or hundreds of iterations.

Natural fault populations commonly show one order of magnitude spread in length for a given T_{max} (as observed by Cartwright et al., 1995). We believe, as they do, that this variation is a consequence of repeated coalescence or linkage of *growing* faults that have not all reached the steady-state growth line. Due to continued interaction and coalescence, steady-state growth may not be a typical, attainable state of fault growth at all.

SANDBOX MODELS – EXPERIMENTAL PROCEDURE

Here, we describe results from a single, plane strain experiment (Figure 2) that was followed through time, at successive strain increments as well as supplementary experiments conducted under an X-ray tomograph to study the 3-D propagation of fault slip surfaces (Figure 3). Measurements of fault length, vertical offset and displacement profiles at the surface of the sand-pack were made from digital laser-scans (with a vertical resolution of 50 μm) of the faulted sand surface.

The sandbox models consisted of a 2.4 cm sand layer (0.1 mm grain size) overlying a layer of low viscous putty 0.8 cm thick. The sand is a good analogue for modelling the brittle behaviour of upper crustal rocks (Horsfield, 1977; Vendeville et al., 1987; Richard and Cobbold, 1990). The putty used is a good analogue to model the ductile behaviour of salt in the upper crust. Although a discussion of the experimental scaling is beyond the scope of this paper, the models were scaled using methods discussed by Hubbert (1937), Ramberg (1967), Vendeville et al., (1987) and Richard (1991).

Homogeneous plane strain extension was applied to the model by stretching a rubber sheet beneath the putty layer (Figure 2) at a constant velocity (2.5 cm/hr). Scaling is such that 1 cm in the model represents about 1 km in nature and the strain rate is equivalent to 2 cm/yr at crustal scale.

The sand and putty thicknesses were chosen (based on a series of pilot experiments) in order that a substantial number of faults develop in the sand but few enough to permit detailed observations. The layer of putty was placed at the base of the model to initiate faulting at the free surface of the sand-pack; thus, the maximum vertical throw accommodated by the faults is the offset measured at the free surface of the sand-pack. The experiment was conducted with increasing strains up to 6%.

FAULT INITIATION

As the sand-pack is extended, minimum horizontal stress decreases and the sand initially dilates by adjustment of the position of sand grains relative to one another. After about 1% strain (Figure 3), dilation becomes concentrated onto several narrow segments, or fault seeds, which

appear to be randomly distributed over the surface of the sand. The development of these narrow zones of dilation was monitored by X-ray tomography in 3-D, in separate, preliminary experiments in both time and space (Figure 3). The population of faults observed both on the sand-pack surface and in 3-D decreases with strain and a smaller number of faults than were observed shortly after initial stretching eventually accommodate vertical offset as strain increases. On the sand surface, the zones of dilation develop into relatively long, straight and narrow segments with little or no displacement initially and limited vertical penetration into the sand-pack at first. The L/T_{max} ratios at this stage have not been measured because the displacement is so low. However, the L/T_{max} ratio for these fault segments is probably very large and in excess of 200. We believe that these segments are formed when fault seeds on a scale of a few sand grains rapidly coalesce in a dilation zone to form a single, coherent segment. Many of the earlier, dilated segments return to a density and porosity that is indistinguishable from the matrix and become invisible on the X-ray scans.

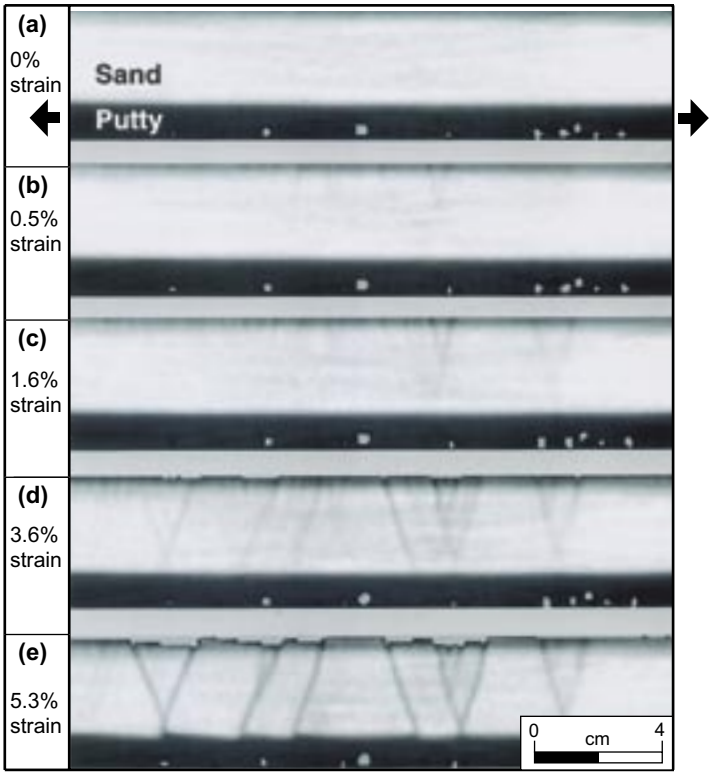

Figure 3: Sequence of fault development in cross-section in a sandbox model, scanned by X-ray tomography. By 3.6% strain (d), distinct faults with 1 to 2 mm vertical offset have developed. By 5.3% strain (e), the 'conjugate' faults also offset the base of the sandpack at the interface with the putty layer. The deformed sand layer now has the appearance of tilted fault blocks with a horst (at centre) and graben structure.

GROWTH OF A COALESCED FAULT

We shall illustrate the process of fault growth after coalescence of fault segments by following the development of a particular set of faults.

At 2.5% strain (Figure 4a), the highlighted fault array in surface view is composed of three distinct, separate segments. By 3% strain (Figure 4b), the fault segments have grown towards each others and have formed a single, coalesced fault. At this stage, the fault population is composed of both single and coalesced faults. This sandbox fault population is very similar to the set of faults observed in the Natih Formation on the southern flank of Al Jabal al Akhdar (Figure 4c). This analogue is used to aid fault interpretation in the sub-surface e.g. based on seismic data.

At 3% strain, the highlighted fault has a serrated and segmented profile (Figure 5a) and a high Length to Maximum Throw ratio (L/T_{max} = 155). The three originally separate segments, fs1 to fs3, are still recognisable on the surface view (Figure 4) but have been joined and connected by two additional fault segments, fs4 and fs5 (Figure 5a). The individual segments can be identified on the fault throw profile by displacement minima (Figure 6a). In many cases of coalescence, the fault segments are offset laterally from each other. At the point of coalescence, the fault tips slightly overlap. Then the overlap zone or relay is breached.

From 3 to 4.2% strain, the coalesced fault has grown (Figure 5b), but has accommodated proportionately more vertical displacement than a corresponding increase in length. As a result, the L/T_{max} ratio decreased to 73. Its throw profile is serrated and throw minima clearly mark the positions of the earlier separate fault segments (Figure 6b).

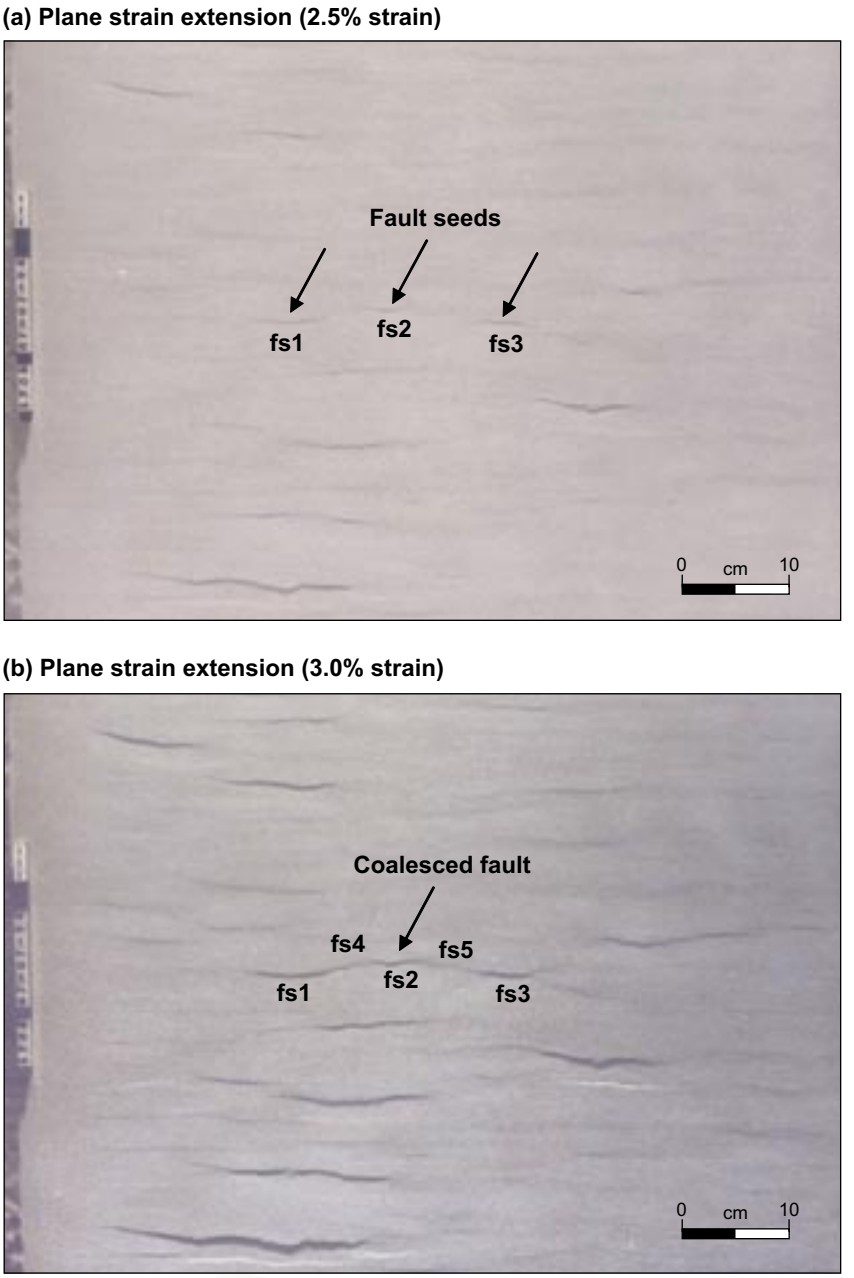

Figure 4: Surface view of sandbox at (a) 2.5% and (b) 3.0% extensional strain. Note the development of significantly longer, coalesced faults from earlier faults seeds (See Figures 5a and 6a). (c) Oblique view of southern flank of Al Jabal al Akhdar, Oman, based on aerial photograph montage draped over Digital Elevation Model. Selected fault breaks are indicated by black arrows, fault tips by orange arrows. Wadis form incisions down slope generally oriented perpendicular to the fault segments. The faults have offsets reaching 80 m and cut through the top of the upper Cretaceous Natih Formation (dominantly limestone with some shales).

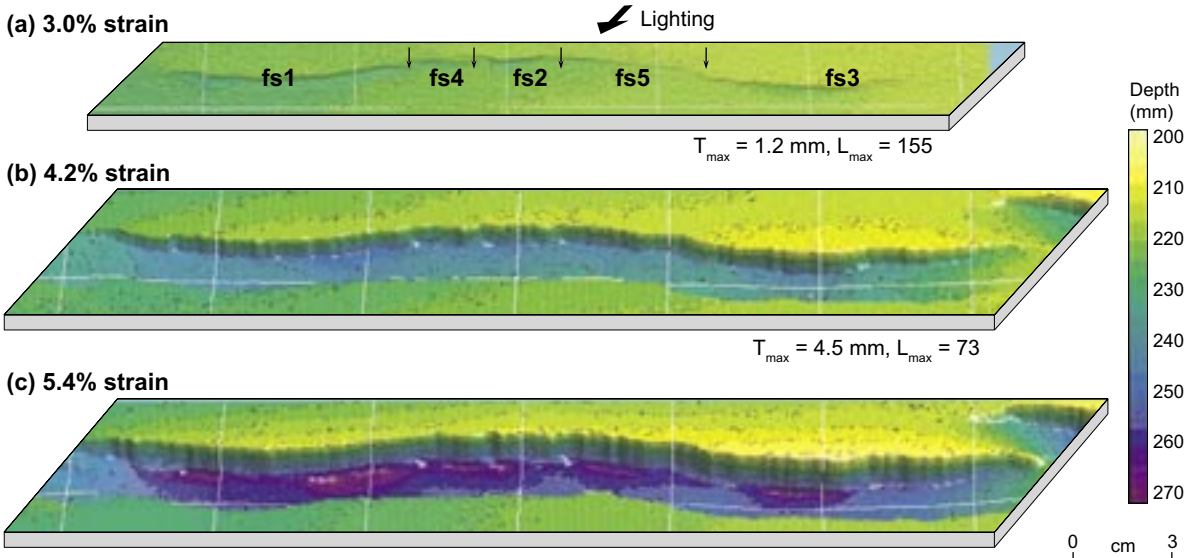

Figure 5: Sequential growth of a coalesced fault in sandbox model of plane strain extension.

(a) At 3% strain, fault coalescence just took place and initially separate segments are still recognisable as local deep areas (in dark green). The black arrows indicate the approximate position of the fault segment tips (see Figure 6a for precise location).

(b) After 4.2% of strain, the fault has increased marginally in length, and substantially in displacement. Both tips begin to overlap with nearby faults in relay zones

(c) From 4.2 to 5.4%, the fault accumulated mainly vertical displacement. Its tips are locked at relays where throw gradient increased (Figure 6c). After increasing strain, the early separate segments are still recognisable along the graben as local deeps.

From 4.2 to 5.4% strain, the fault accumulated vertical displacement at its centre. There was no significant increase in length observed (L/T_{max} = 55, Figures 5c and 6c). Both lateral tips interact with other faults in relays and, as a consequence of this interaction, the throw gradient increased at both tips. The magnitudes of the throw minima are constant through time but become relatively small compared to the growing central maximum throw of the coalesced fault. The final fault trace, as viewed on a map, is arcuate (Figure 5c). At these relatively high strains, few faults (about 20% of the population) remain isolated and these tend to be located at the edge of the sand-pack where boundaries do not permit coalescence at one of the tips.

MODIFICATION OF FAULT POPULATION SLOPES WITH INCREASING STRAIN

Once a fault pattern is well established, after 3 to 4% strain, it appears that few new faults are added to the population to follow the growth trajectory described above. Thus, strain in the sand-pack is accommodated on existing faults. The large faults (over 10 cm long) accommodate a greater proportion of strain than smaller faults. However, the shorter faults (3 to 10 cm long) continue to grow by lateral tip propagation and by coalescence.

With increasing strain, from 4.2 to 5.4%, the slope of the best fit regression line to the fault population of L vs T_{max} increased from 1.0 to 1.3 (Figure 7). During this increment of strain, several faults were monitored to determine how individual faults grow. Their growth vectors (i.e. change in L and T_{max}) plotted on double log space have slopes that are generally greater than 1.5 (Figure 8).

FAULT POPULATIONS IN NORTH OMAN

Here we describe the geometric character of faults exposed at the surface on the southern flank of Al Jabal al Akhdar in north Oman and draw analogies between faults observed in the subsurface and in

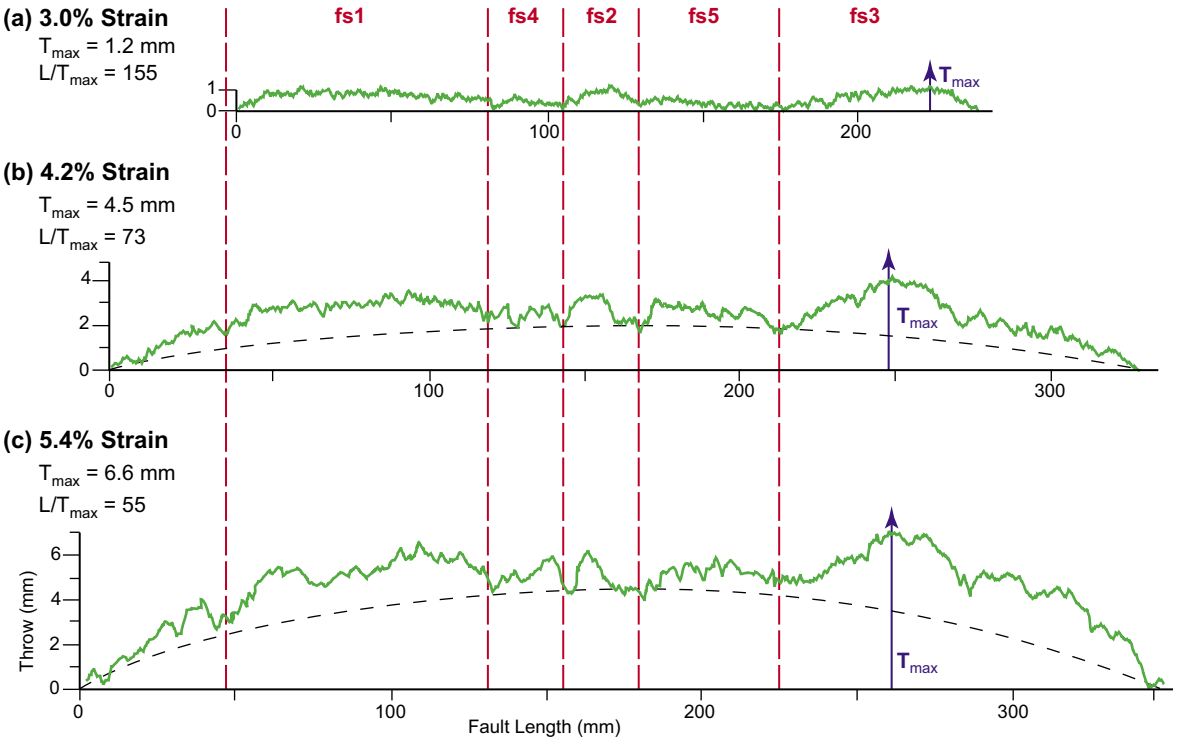

Figure 6: Sequential fault throw profiles of a coalesced fault in a sandbox model of plane strain extension. Fault throw profiles were analysed using data from the videolaser scan and proprietary software.

(a) At 3% strain, the fault displayed resulted from the coalescence of early separate segments fs1, fs2 and fs3 which are recognisable as throw minima (dashed vertical lines) on the serrated throw profile. The maximum throw was accommodated by the right-hand segment.

(b) From 3 to 4.2% strain, the fault has grown marginally in length but substantially in displacement. The length / throw ratio decreased from 155 to 73.

(c) From 4.2 to 5.4% strain, the fault behaves as a single fault and accumulated vertical displacement at its centre (dashed arcuate line). However, the fault increased only slightly in length (L/T_{max} = 55) and, as a result of slower lateral tip propagation, throw gradient increased at both tips. The magnitude of the throw minima becomes relatively small with time compared to the maximum throw on the fault. With increasing strain, the position of the maximum fault throw (arrowed) remains more or less fixed.

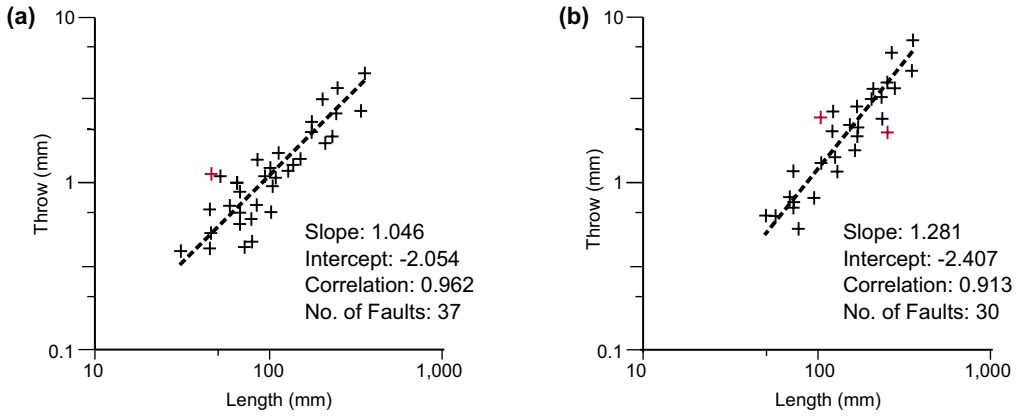

Figure 7: Length and T_{max} data for faults from the same sandbox experiment at different strains. The slope of the best fit regression line is (a) 1.046 at 4.2% strain and (b) 1.281 at 5.4% strain. Large faults accumulate proportionately more throw than increase in length. Red crosses indicate that the fault lies outside the 95% confidence limit for the regression.

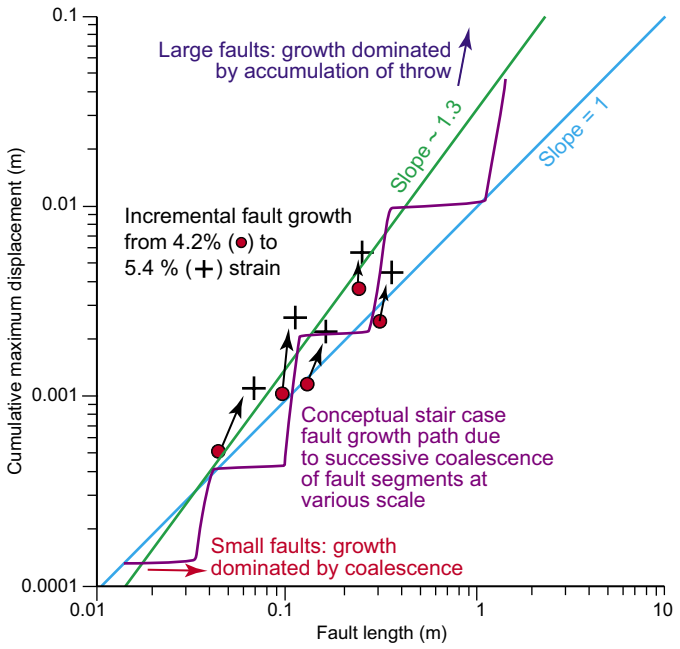

Figure 8: Conceptual staircase model for fault growth. Incremental fault growth follows a steep path (slopes in log space greater than 1.5). However, the slope of the best fit regression lines to the fault population at successive stages of strain steepens from about 1.0 to 1.3. This is because, initially, small faults tend to grow by coalescence and reach a given length and after coalescence large faults tend to accumulate more displacement but increase in length at a slower rate. The larger faults in the population accommodate an increasing proportion of strain. Through successive coalescence a given fault follows a staircase growth profile.

the sandbox models. The late Cretaceous faults are located in the footwall of thrusts that carried the Semail Ophiolite southwards during the Turonian and Santonian (Cooper, 1988). The thrusts carried the emplaced ophiolite as well as basin, slope and platform carbonates southwards over a distance in excess of 400 km and eventually buried the Natih and Fiqa formations to a depth of at least 5 km on Al Jabal al Akhdar, based on reconstructions by e.g. Cooper (1988) and Hanna (1990). Although the sedimentary facies of the Natih carbonates on Al Jabal al Akhdar are similar to those found in the subsurface some 50 to 100 km to the south, reservoir properties have been substantially overprinted by compaction and cementation soon after the faults formed and after burial below the thrust sheets. The population of faults described here formed as a result of oblique collision with the Indian Plate imparting a NW-SE oriented maximum horizontal stress and developed prior to burial by the south-verging thrust sheets (Filbrandt et al., 2006). Maximum stress is interpreted to have been vertical. The faults closely resemble those mapped in the subsurface from the Natih to the Gharif formations on 3-D seismic data (Figures 9 and 10). The southern flank of Al Jabal al Akhdar was tilted to its present position during the later part of the Tertiary as a result of NE-SW oriented collision with the Iranian Plate. Although we believe the faults developed with a minor strike-slip component, the fault families exhibit similar characteristics to those observed in the sand box experiments.

The dominant fault population comprising faults oriented E-W to WNW-ESE on the southern flank of Al Jabal al Akhdar (Figure 4c) displays geometric similarities to those observed propagating in the sand box models (Figures 4a and 4b) in terms of fault throws and lengths. The faults were assessed using a combination of georeferenced aerial photographs and a detailed digital elevation model (DEM) at a scale of 1:15,000 and absolute vertical resolution of a few tens of centimetres, but with higher lateral resolution. The best fit regression line to the L/T_{max} population of the faults on Al Jabal al Akhdar is 0.88 (Figure 11). However, we stress that the L/T_{max} analyses extracted from surface outcrops must be considered with care due to the erosion of the dip-slope of Al Jabal al Akhdar. The dip slope is formed at the interface between the easily eroded, shale-prone Fiqa Formation and the carbonates at top Natih level. The Natih Formation is also eroded up-slope as far as the Nahr Umr and Shu'aiba formations, a stratigraphic thickness of some 500 m over a distance of 5 to 7 km. Nevertheless, in the footwall, limestone beds can be traced in the fault scarp or walked for several hundred metres and occasionally kilometres. Thus, the shape of the fault throw profile is faithfully preserved in the digital elevation model (DEM) if not the maximum fault throw. Fault populations mapped in the subsurface in the Cretaceous carbonates equivalent to those observed on Al Jabal al Akhdar should have broadly similar L/T_{max} population slopes.

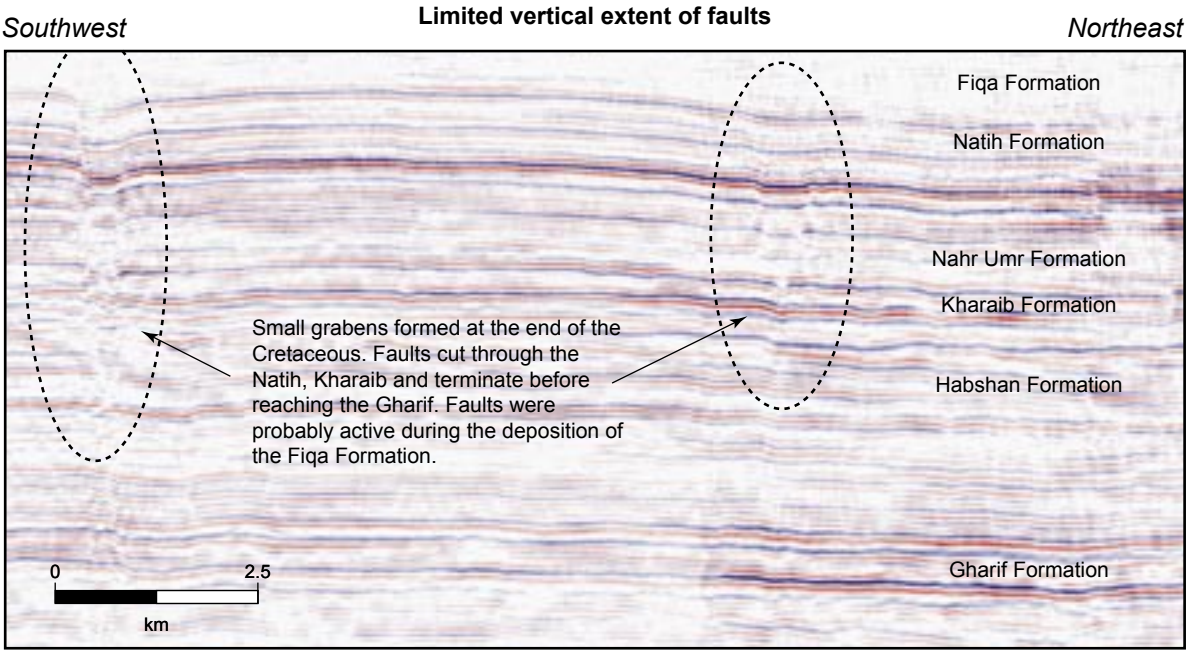

Figure 9a: Seismic section illustrating the nature of the fault sets in the Mesozoic carbonate platform sediments. Faults are steep, extending from the Fiqa Formation through to the Gharif Formation, but rarely enter the Haima Supergroup sediments. Often the faults form in pairs (bounding narrow grabens) and the fault intersection marks the limit of displacement either in the Mesozoic carbonates, i.e. Natih, Kharaib, Habshan formations or in the Gharif Formation (Filbrandt et al., 2006).

Although the footwalls are partially eroded, the profiles of the faults on Al Jabal al Akhdar and in the sub-surface are typically segmented (compare Figures 12a and 12b with Figures 6a to 6c). In addition, examples of overlapping faults with relays as well as coalesced faults based on the fault throw profiles are evident. They are inferred to have evolved in a similar fashion to those in the sand box by propagation and coalescence. Throw minima which occur towards the centre of the profile are relatively small compared to the neighbouring maxima of coalesced segments (e.g. Figure 12a, Fault A).

DISCUSSION

In the sandbox experiments discussed, the initial, sand-grain-scale fault seeds are randomly distributed at first, but soon develop into linear arrays (Figure 1c). The separation of the arrays parallel and perpendicular to the strike of the faults appears to be controlled by instabilities in the sand-pack. The fact that linear arrays of fault seeds form suggests that fault growth is initially dominated by coalescence of very small fault seeds and subsequent rapid accumulation of displacement at an early stage. With increasing strain, the fraction of small faults becomes less important in terms of the amount of strain accommodated by these faults, either because they grow by lateral tip propagation or they coalesce. The total number of faults does not remain constant with increasing strain and the decline in numbers caused by coalescence is not made up by "newly-born," smaller faults.

At the moment of coalescence, the through-going, linked fault segment may be several times longer than any of its constituent segments (as observed in the fault systems described by Cartwright et al., 1995). Once coalesced, the linked segments behave as a single fault (Meyer et al., 2002) with more displacement accumulating near the centre of the fault than at the fault tips (Figure 6). Lateral fault propagation decelerates and fault tips remain almost stationary (Morewood and Roberts, 2002; Cowie and Roberts, 2001). The throw profile becomes flatter with increasing strain, possibly because the fault can no longer accommodate displacement. At this point in our model, the fault reaches the base of the sand layer and may be equivalent to a fault reaching a shale or salt layer: compare our observations from outcrop and sub-surface data, e.g. from the top of the Natih Formation to the Nahr Umr shale, some 400 to 500 m below, for faults two to four kilometres long at the Natih-Fiqa shale interface.

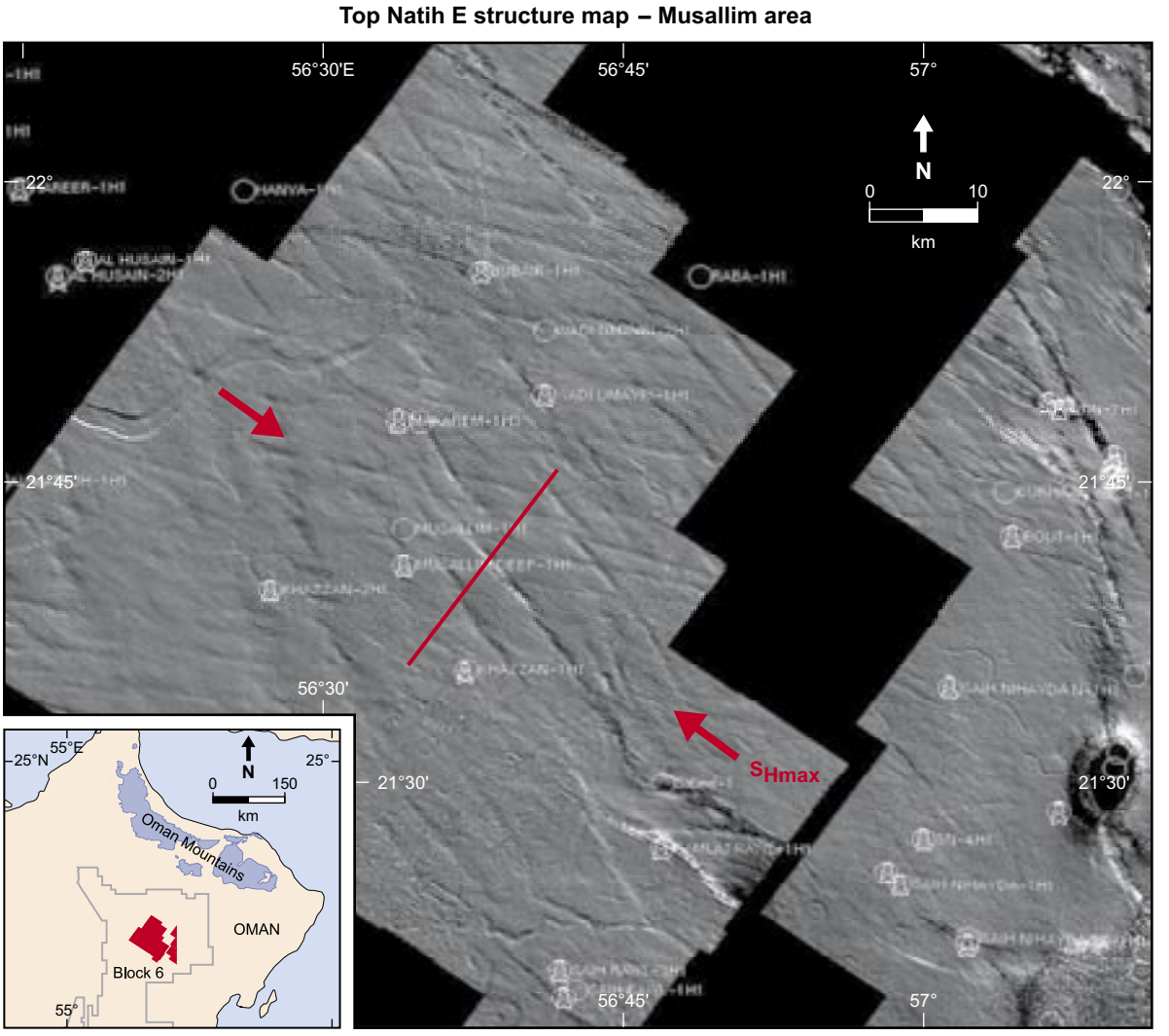

Figure 9b: Surface illumination map at Natih E level from the Musallim-Makarem slope. Two fault sets are equally well-developed suggesting the maximum horizontal stress at the time of the formation of the faults was oriented NW-SE (Filbrandt et al., 2006).

In summary, the progress of fault growth follows the following stages:

(1) early development of grain-scale fault seeds;
(2) formation of linear arrays of fault seeds into coherent fault segments;
(3) growth by displacement and tip propagation;
(4) fault coalescence by relay breaching and connection to adjacent fault segments; and
(5) connected fault segments accommodate displacement near centre of profile and behave as a single fault.

The last three stages (3 to 5 above) continue the sequence of fault evolution by cyclic repetition of growth and coalescence.

This fault growth by repetitive coalescence has potentially an important implication on the fault damage zone model. The faults tend to reach a given length rapidly, then accommodate throw with

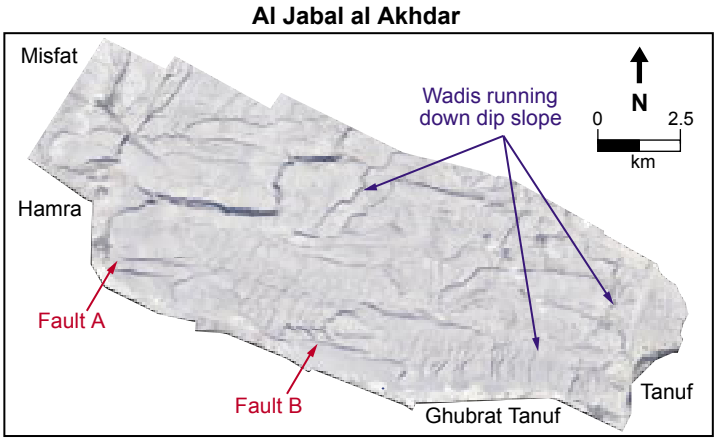

Figure 10: Aerial photograph of fault planes intersecting the top of the Natih Formation on the southern slopes of Al Jabal al Akhdar. The faults cut down from the top of the Natih Formation to the base of the Mesozoic carbonate section. (For further discussion see Filbrandt et al., 2006, figures 34 to 36).

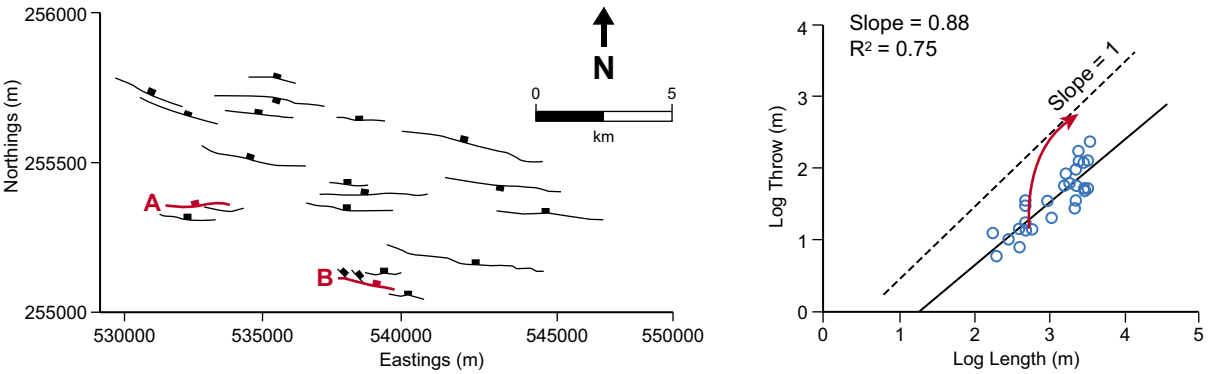

Figure 11: Length and T_{max} data for the fault population from Al Jabal al Akhdar with best fit regression line slope of 0.88. Lengths and throws have been measured from digital elevation model data over Al Jabal al Akhdar. However, erosion of the footwalls and fault tips results in some uncertainties in both these measurements.

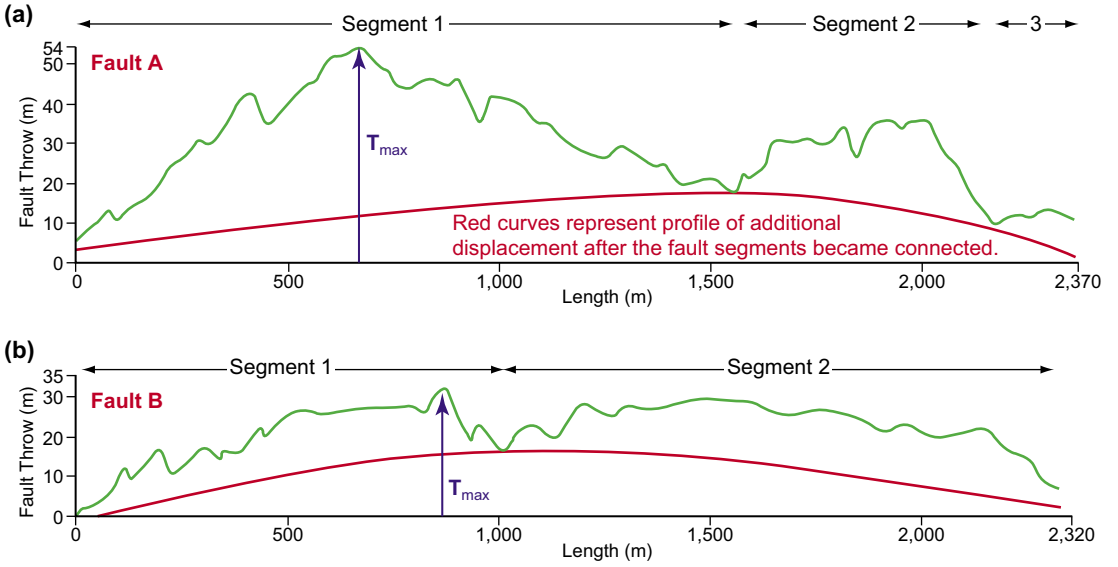

Figure 12: (a) and (b) Fault throw profiles of two faults from the SW flank of Al Jabal al Akhdar. Locations of the faults are highlighted in Figure 10 and extracted from the digital elevation model for Al Jabal al Akhdar. Throw on the Y-axis and length on the X-axis are measured in metres.

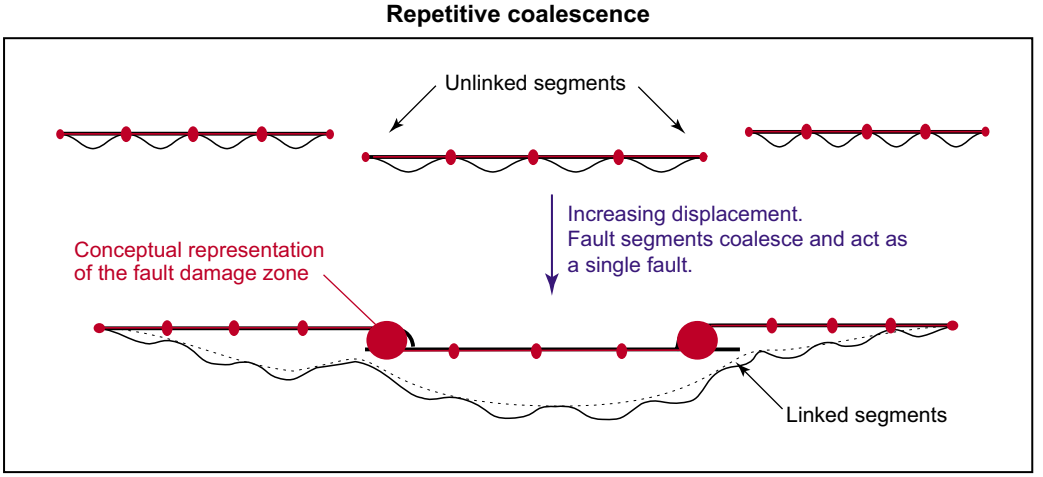

Figure 13: Fault damage zone concept of coalesced faults. The relay zones represent areas where the damage zone is wider (red areas) while the throw is minimum. The damage zone is narrower where the throw reaches a maximum away from relay zones. With increasing strain (accommodation of displacement), the damage zone increases mainly by breaching of the relay zones at new coalescence points (largest red areas).

minor fault tip propagation until the next coalescence event. The relay zones represent areas where the damage zone is wide while the throw is near its minimum (Figure 13). The damage zone is narrower where the throw is at a maximum away from relay zones (Figure 13). This model supports the concept proposed by Kim et al. (2004), and contrasts with the conclusions of Shipton and Cowie (2003).

The gradient of the best-fit regression lines to L/T_{max} data for the fault populations in these sandbox experiments at relatively high strains is close to or slightly greater than one, i.e. as steady-state growth is approached. This lends support to the linear growth model proposed by e.g. Cowie and Scholz (1992) based on similar fit of regression lines to fault populations from theoretical models. However, we observed that the incremental growth is much steeper than one for both coalesced and isolated faults. Thus, we believe that growth models based on analysis of static populations do not adequately describe growth processes. Faults actually appear to grow by a combination of coalescence and rapid accumulation of throw. These processes occur at all scales and, with increasing strain, reach and help to maintain a population slope of about one.

Our numerical models do not show this dynamic effect in the change of the population slope but highlight that faults accommodate displacement rapidly if "under-displaced" after coalescence as suggested by Cartwright et al. (1995) or after initial rupture of the rock volume. Although our experimental data suggest that the population slope is about one, the validity of this value for all fault populations is still uncertain. This is because a given normal fault population may not have reached steady-state at the time that extension ceased. The process of coalescence always tends to steepen the L/T_{max} slope particularly in closely spaced fault populations. The greater the initial fault spacing, the greater the chance individual faults have to grow towards steady-state without encountering or coalescing with another fault. Coalescence causes a sudden increase in fault length resulting in a move to the right in L/T_{max} space. After coalescence, accommodation of displacement out-strips the rate at which faults propagate and the fault tracks a steep path in L/T_{max} space. Lateral fault tip propagation gradually becomes more important as the coalesced fault approaches the "steady-state" growth line (cf. Walsh et al., 2002).

CONCLUSIONS

The sandbox experiments discussed in this paper have a direct implication for sub-surface interpretation of oil reservoirs in Oman. This has been illustrated with the analogy between sandbox and outcrop fault geometries of the Natih Formation of Al Jabal al Akhdar. Wider physical (and

possibly also chemical) fault damage zones with higher fracture densities are expected near linked fault segments, indicated by lows or in the fault throw profile that can be mapped on 3-D seismic. In these sandbox experiments normal faults appear to grow by repetitive coalescence of fault segments at all scales. After each coalescence event, the L/T_{max} ratio increases temporarily. A chain of linked segments behaves as a single fault and accumulates more displacement at its centre, faster than increasing in length, thus reducing the L/T_{max} ratio.

After a large number of growth increments, and no further coalescence, the new linked fault may reach a steady-state growth curve with a population L/T_{max} slope of about 1 to 1.3. Repeated coalescence of "under-displaced," growing faults explains a large part of the observed spread in L/T ratios. Incremental growth of individual faults has a slope in L/T_{max} space that is greater than 1.5. Initially, separate segments remain recognisable by throw minima of constant magnitude with increasing strain, but become relatively small compared to the eventual maximum throw of the fault.

ACKNOWLEDGEMENTS

We gratefully acknowledge and thank Shell International for permission to publish this paper. This paper builds on a research program undertaken at the Research Laboratories of Shell International in Rijswijk, The Netherlands during the mid 1990s. We would sincerely like to acknowledge the contribution made by Akke-Marijke Gunst for her contribution to the sandbox modelling work. We are indebted to Mike Naylor, Jilles van den Beukel, Ramon Loosveld, Chris Jones, Gary Ingram, Leo Zijerveld, Dick Nieuwland and Jacquie Fulljames for discussions in developing these concepts. We thank the Ministry of Oil and Gas in Oman for approval to use the references to Al Jabal al Akhdar and permission to use displays of seismic data. The final design and drafting of graphics by Gulf PetroLink is appreciated.

APPENDIX

Derivation of incremental growth models: the basis for simulating fault growth. The derivation of an incremental growth model is largely based on the generalised approach presented in Cowie and Scholz (1992). From seismological studies, the mean slip during the n^{th} seismic cycle, $T_{mean,n}$ is found to be related to the length of the rupture Cowie and Scholz (*op. cit*.). Assuming that the entire fault surface is ruptured in each seismic cycle (contrast with Shipton and Cowie, 2003), the mean slip is related to the existing fault length, L_{n-1}:

$$\Delta T_{mean,n} = \alpha L_{n-1} \quad \textbf{(Equation 1)}$$

Where α is found to be between about 1.5×10^{-5} and 6×10^{-5}. For elliptical and triangular displacement profiles respectively along a fault trace, it can be shown that:

$$\Delta T_{mean} = 0.8 \Delta T_{max}$$
$$\Delta T_{mean} = 0.5 \Delta T_{max}$$

An ellipticity of 2:1 has been modelled in this analysis. The cumulative displacement, $T_{max,n}$ after n seismic cycles can be derived from Equation 1 as follows:

$$T_{max,n} = \sum_{i=1}^{n} \Delta T_{max,i} = \alpha' \sum_{i=1}^{n} L_{i-1} \quad \textbf{(Equation 2)}$$

where α' is 1.25α and 2α for elliptical and triangular displacement profiles respectively. If we assume an empirical power-law relation between fault length and each new length increment, we can write:

$$\Delta L_i = r(L_{i-1})^{\beta} \quad \textbf{(Equation 3)}$$

where *r* and β are constants. β is related to the power-law exponent of the steady-state growth law (see main text) according to $\beta = 2 - C$. For example, in the particular case of $\beta = 0$, we have:

$$\Delta L = r \quad \textbf{(Equation 4)}$$

And C = 2, which represents the model proposed by Walsh and Watterson (1992). Combining Equation 3 into Equation 2:

$$T_{\max,n} = \frac{\alpha}{r^{1/\beta}} \sum_{i=1}^{n} (\Delta L_i)^{1/\beta} \qquad \textbf{(Equation 5)}$$

Where ΔL is the increase in fault length during the n^{th} seismic cycle. Equation 5 can be re-written to relate slip increment to length increment as follows:

$$\Delta T_{\max,n} = T_{\max,n} - T_{\max,n-1}$$

$$\therefore \Delta T = \frac{\alpha}{r^{1/\beta}} \left[\sum_{i=1}^{n} (\Delta L_i)^{1/\beta} - \sum_{i=1}^{n-1} (\Delta L_{i-1})^{1/\beta} \right] \qquad \textbf{(Equation 6)}$$

$$\therefore \Delta T = \frac{\alpha}{r^{1/\beta}} \Delta L_n^{1/\beta}$$

Fault growth and displacement evolution are modelled by iterating Equations 1, 3, 4 and 6 for n increments, usually in the hundreds.

REFERENCES

Cartwright, J.A., B.D. Trudgill and C.S. Mansfield 1995. Fault growth by segment linkage – an explanation for the scatter in maximum displacement and trace length data from the Canyonlands grabens of SE Utah. Journal of Structural Geology v. 17, p. 1319-1326.

Cooper, D.J.W. 1988. Structure and sequence of thrusting in deep-water sediments during ophiolite emplacement in the south-central Oman Mountains. Structural Geology, v. 10, p. 473-485.

Cowie, P.A. and G.P. Roberts 2001. Constraining slip rates and spacings for active normal faults. Journal of Structural Geology, v. 23, p. 1901-1915.

Cowie, P.A. and C.H. Scholz 1992. Growth of faults by accumulation of seismic slip. Journal of Geophysical Research, v. 97, p. 11085-11095.

Filbrandt, J.B., R.C.M.W. Franssen and P. Richard 1995. Fault evolution in sandbox experiments. Abstract, Edinburgh Conference, Tectonic Studies Group.

Filbrandt, J.B., S. Al-Dhahab, A. Al-Habsy, K. Harris, J. Keating, S. Al-Mahruqi, S.I. Ozkaya, P.D. Richard and T. Robertson 2006. Kinematic interpretation and structural evolution of North Oman, Block 6, since the Late Cretaceous and implications for timing of hydrocarbon migration into Cretaceous reservoirs. GeoArabia, v. 11, no. 1, p. 97-140.

Hanna, S.S. 1990. The Alpine deformation of the central Oman Mountains. In, A.H.F. Robertson, M.P. Searle and A.C. Ries (Eds.), The Geology and Tectonics of the Oman Region. Geological Society of London, Special Publication no. 49, p. 341-359

Horsfield, W.T. 1977. An experimental approach to basement controlled faulting. Geologie in Mijnbouw, v. 56, no. 4, p. 363-370.

Hubbert, M.K. 1937. Theory of scale models as applied to the study geologic structures. Geological Society of America Bulletin, v. 48, p. 1459-1520.

Johnson, C.A., T. Hauge, S. Al-Menhali, S. Bin Sumaidaa, B. Sabin and B. West 2005. Structural styles and tectonic evolution of onshore and offshore Abu Dhabi, UAE. International Petroleum Technology Conference Doha (IPTC 10646), p. 1-15.

Johnson, C.A. and S. Agar 2004. Structural characterization of carbonates in the United Arab Emirates: from regional to reservoir scale. 6th Middle East Geosciences Conference, GEO 2004. GeoArabia, Abstract, v. 9, no. 1, p. 84.

Kim, Y.-S., D.C.P. Peacock and D.J. Sanderson 2004. Fault damage zones. Journal of Structural Geology, v. 26, p. 503-517.

Lange, S., J. Mattner and J. Teasdale 2006. Structural evolution of the Wajid area, Western Rub' Al-Khali Basin, Saudi Arabia. 7th Middle East Geosciences Conference, GEO 2006, Abstract.

Marrett, R. and R.W. Allmendinger 1990. Kinematic analysis of fault-slip data. Journal of Structural Geology, v. 13, p. 735-737.

Meyer, V., A. Nicol, C. Childs, J.J. Walsh and J. Watterson 2002. Progressive localisation of strain during the evolution of a normal fault population. Journal of Structural Geology, v. 24, p. 1215-1232.

Morewood, N.C. and G.P. Roberts 2002. Surface observation of active normal fault propagation: implications for growth. Journal of the Geological Society, v. 159, p. 263-272.

Ramberg, H. 1967. Gravity, Deformation, and the Earth's Crust. Crust Academic Press, New York, NY, 214 p.

Richard, P.D. 1991. Experiment on faulting in a two-layer cover sequence overlying a reactivated basement fault with oblique-slip. Journal of Structural Geology, v. 13, no. 4, p. 459-469.
Richard, P.D. and P.R. Cobbold 1990. Experimental insights into partitioning of fault motions in continental convergent wrench zones. Annales Tectonicae, Special Issue IV, no. 2, p. 35-44.
Sercombe, W.J., I.P. Saxby and T.S. Al-Failakawi 2004. Revised structural interpretation of Sabiriyah field, Kuwait. 6th Middle East Geosciences Conference, GEO 2004. GeoArabia, Abstract, v. 9, no. 1, p. 130.
Shipton, Z.K. and P.A. Cowie 2003. A conceptual model for the origin of fault damage zone structures in high porosity sandstone. Journal of Structural Geology, v. 25, p. 333-344.
Tamura, Y., F. Tsuneyama, H. Okamura and K. Furuya 2004. Fault characterization by seismic attributes and geomechanics in a Thamama oil field, UAE. GeoArabia, v. 9, no. 2, p. 63-76.
Vendeville, B., P.R. Cobbold, P. Davy, P. Choukroune and J.P. Brun 1987. Physical models of extensional tectonics at various scales. In, M.P. Coward, J.F. Dewey and P.L. Hancock (Eds.), Continental Extensional Tectonics. Geological Society of London, Special Publication no. 28, p. 95-108.
Walsh, J.J., A. Nicol and C. Childs 2002. An alternative model for the growth of faults. Journal of Structural Geology, v. 24, p. 1669-1676.
Walsh, J.J. and J. Watterson 1992. Populations of faults and fault displacement and their effects on estimates of fault-related regional extension. Journal of Structural Geology, v. 14, p. 701-712.
Watterson, J. 1986. Fault dimensions, displacements and growth. Pure and Applied Geophysics, v. 124, p. 365-373.
Webb, S., D. Cassiani, J. Mariano and A. Al-Ateeqi 2000. Tectonostratigraphic evolution of the Gotnia Basin, Kuwait. 4th Middle East Geosciences Conference, GEO 2000. GeoArabia, Abstract, v. 5, no. 1, p. 197.

ABOUT THE AUTHORS

Jacek B. Filbrandt *is currently at Shell Petroleum Development Company in Port Harcourt, Nigeria working on fault seal capacity in traps of the Tertiary deltaic sequence. He has a BSc in Earth Sciences from Leeds University and a PhD in Structural Geology and Geophysics from University College, Cardiff. Jacek joined Shell Expro in 1985 working mainly on 3-D seismic surveys in the appraisal division. He subsequently moved to Shell International EP in The Netherlands and worked in New Ventures with responsibility for developing greenfield opportunities, mainly in East Africa and the Middle East. He was a member and leader of the Structural Geology Team at Shell Research in the mid 1990s. Jacek spent three years with Shell Oil in New Orleans, exploring the deepwater Sub-Salt Play. He joined Petroleum Development Oman in 1999 and was head of the Structure and Traps team.* *jacek.filbrandt@shell.com*

Pascal D. Richard *is a Senior Structural Geologist in the Study Centre of Petroleum Development Oman (PDO). He has a PhD in Structural Geology on strike-slip tectonics from the University of Rennes, France. Pascal joined Shell in 1991. He spent 4 years in the research structural geology department working on modelling of structural styles, fault growth and hydrocarbon systems. After 3 years in PDO as Structural Geology Consultant and Seismic Interpreter, Pascal worked 5 years in Shell EP research Carbonate Development Team focusing on the characterisation and modelling of fractured reservoirs. Since 2003, Pascal has been implementing fracture technology in PDO, and has a role in coaching and knowledge transfer. Pascal is also a global expert for Shell in structural geology.*
pascal.richard@pdo.co.om

Raymond Franssen *currently is the Principle Explorationist in Southeast Asia. He received a PhD from Utrecht University, The Netherlands, and joined Shell Exploration and Production in 1989. Raymond has had assignments in research, production and exploration in The Netherlands, USA, Egypt and Malaysia. His main professional interests are play and prospect evaluation combined with effective delivery of business opportunities that lead to the discovery of hydrocarbons.*
raymond.franssen@shell.com

Manuscript received March 2005; Revised September 14, 2005
Accepted June 4, 2006; Press version proofread by authors November 20, 2006